# The acidic nature of "NMR-invisible" tri-coordinated framework aluminum species in zeolites

Shaohui Xin, Qiang Wang, Jun Xu, Yueying Chu, Pengfei Wang, Ningdong Feng, Guodong Qi, Julien Trebosc, Olivier Lafon, Weibin Fan, et al.

# Acidic Nature of "NMR-invisible" Tri-coordinated Framework Aluminum Species in Zeolite†

Shaohui Xin,[ad] Qiang Wang,*[a] Jun Xu,[a] Yueying Chu,[a] Pengfei Wang,[b] Ningdong Feng,[a] Guodong Qi,[a] Julien Trébosc,[c]

Olivier Lafon,[ce] Weibin Fan[b] and Feng Deng*[a]

[a.] National Centre for Magnetic Resonance in Wuhan, State Key Laboratory of Magnetic Resonance and Atomic and Molecular Physics, CAS Key Laboratory of Magnetic Resonance in Biological Systems, Wuhan Institute of Physics and Mathematics, Chinese Academy of Sciences, Wuhan 430071, China. E-mail: qiangwang@wipm.ac.cn; dengf@wipm.ac.cn

[b.] State Key Laboratory of Coal Conversion, Institute of Coal Chemistry, Chinese Academy of Sciences, P.O. Box 165, Taiyuan, Shanxi 030001, P. R. China

[c.] Univ. Lille, CNRS, ENSCL, UMR 8181, Unité de Catalyse et de Chimie du Solide 59000 Lille, France

[d.] University of Chinese Academy of Sciences, Beijing 100049, China

[e.] Institut Universitaire de France, 75231 Paris, France

Unambiguous characterization of different acid sites in zeolites is of greatimportance for understanding their catalytic performance and rational design of highly efficient zeolite catalysts. In addition to various well-characterized extra-framework Al species, tri-coordinated framework aluminum species can also serve as Lewis acid site in zeolites, which is however "NMR-invisible" due to its extremely distorted local environment. Here we provide a feasible and reliable approach to elucidate the acidic nature of the tri-coordinated framework Al in dehydrated H-ZSM-5 zeolites via sensitivity-enhanced two-dimensional multiple nuclear correlation NMR experiments coupled with trimethylphosphine oxide (TMPO) probe molecules. Two types of tri-coordinated framework Al sites have been unambiguously identified, which amount to 11.6% of the total Brønsted and Lewis acid sites. Furthermore, it is found that the synergistic effect arising from the close spatial proximity between tri-coordinated framework Al site and Brønsted acid site leads to generation of superacidity (with acid strength stronger than 100% $H_2SO_4$) in the zeolite.

## Introduction

Heterogeneous catalysts with acid-base prosperities, such as zeolites have been widely used in chemical and petrochemical industry for catalytic cracking,[1] isomerization,[2] alkylation,[3] and disproportionation.[4] In aluminosilicates-type zeolites, Brønsted acid site (BAS) and Lewis acid site (LAS) are responsible for the active sites in numerous catalytic reactions. Therefore, understanding the structures and properties of the acidic sites in zeolites is essential to explore the reaction mechanism and to optimize their catalytic performance.[5-7] It is well-known that the BAS is associated with the tetrahedral framework aluminum (FAL) in the form of bridging hydroxyl (Si-OH-Al) in zeolites. And the LAS is generally recognized to extra-framework or framework aluminum species, formed upon calcination or steaming of zeolites.[8, 9] The properties of BAS associated with tetrahedral framework Al and LAS associated with various extra-framework Al (EFAL) species have been extensively studied, from their structure characteristics[10-14] to their functions in catalytic reactions.[15-18] Especially, the LAS in zeolite has proved to play an important role in catalytic transformations of hydrocarbons such as hydrogen transfer process,[7, 19, 20] and also generate the Brønsted/Lewis acid synergy owing to the vicinity of corresponding Al species in the local architecture of dealuminated zeolites.[11, 21-23] Although the tri-coordinated FAL is commonly considered as LAS in zeolites, only a few characterizations[24-26] have been attempted to confirm the exsitence of "moisture sensitive" tri-coordinated Al species in zeolite framework. Up to now, no experimental approach has been reported to probe the intrinsic acidic property of such important framework Al species in zeolite.

Solid-state NMR has emerged as an important technique for the characterization of heterogenous catalysts at the atomic scale.[22, 27-31] The coordination state of both FAL and EFAL species in zeolites can be determined on the basis of one-dimensional (1D) [27]Al magic-angle spinning (MAS) and 2D [27]Al multiple-quantum magic-angle spinning (MQMAS) NMR spectroscopy. 2D [1]H-^{1}H and [27]Al-[27]Al double-quantum single-quantum (DQ-SQ) homonuclear correlation MAS NMR methods can provide in-depth structural information on the spatial proximity of different acid sites in dealuminated zeolites,

especially under high magnetic field ( > 18.8 T).[11, 22, 32] Recent report has shown that the perturbed aluminum species was attributed to terminal Al-OH in hydrated zeolites, which was considered to be derived from hydrous tri-coordination of Al species.[33] However, most of these measurements were performed under hydration condition. In the case of non-hydrated zeolites, it is difficult to distinguish FAL species due to the resolution/sensitivity issues from the quadrupolar nature of the $^{27}$Al isotope. The stretch of acidic proton in BAS induces a larger distortion of the corresponding tetrahedral FAL in H-form zeolites, leading to its quadrupolar coupling constants ($C_Q$) up to 14 ~ 18 MHz.[34-36] Generally, mild calcination and dehydration treatments of zeolites would lead to partial breaking (or hydrolysis) of framework ≡Al-O- bond and generation of tri-coordinated FAL and framework silanol group as illustrated in **Scheme 1**.[37-39] Although the neighboring framework Si-OH would interact with the tri-coordinated FAL to restore tetrahedral FAL after cooling down the sample to room temperature, partial Si-OH derived from the breaking of aluminum oxygen bond that bears the proton may be further dehydroxylized with a neighboring defect site (Si-OH group), thus causing an irreversible formation of three-fold coordinated aluminum.[26] However, reducing the number of neighboring oxygen bound to FAL yields a dramatic distortion of its local environment, and the extreme asymmetry of its surrounding electric field results in a

considerable line broadening of its $^{27}$Al NMR resonance (usually with $C_Q$ > 30 MHz).[33, 40] Therefore, the direct observation of tri-coordinated FAL species in dehydrated sample is generally impossible by conventional $^{27}$Al MAS NMR due to its huge quadrupolar broadening and relative low concentration, and the tri-coordinated FAL was suggested to be the "NMR-invisible" species in zeolites.[26, 33] After rehydration, the tri-coordinated FAL could be easily transformed into symmetric tetra-coordinated FAL,[33, 38] which is usually indistinguishable from the FAL of BAS. Further hydrolysis of framework Al-O bond leads to removal of Al from zeolite framework, forming EFAL species such as $Al(OH)_3$, $Al(OH)_2^+$, $AlOH^{2+}$, $Al^{3+}$ and $AlO^+$ etc., which have been well characterized by solid-state NMR spectroscopy.[11, 22, 32, 36, 41, 42]

The adsorption of basic probe molecules such as 2-$^{13}$C-acetone and trimethylphosphine oxide (TMPO) is a feasible approach to investigate the acidity of zeolites.[22, 43-45] The great majority of studies utilized the chemical shift of certain elements (e.g. $^{13}$C or $^{31}$P) in probe molecules to determine the acidic features of zeolites, which were usually combined with density functional theory (DFT) calculations to reveal the relationship between chemical shifts and the corresponding acidic properties (e.g. type, distribution, and strength) on zeolites.[22, 45] However, hitherto it is a great challenge to provide precise and localized information on the structure of the interface between the "guest" probe molecules and the specific acid sites of "host" zeolite via analytical or spectroscopic techniques.

In this contribution, we provide a unique insight into the acidic nature of tri-coordinated FAL species on H-ZSM-5 zeolite by solid-state NMR spectroscopy, and present a clear adsorption picture of TMPO probe molecules on different framework Al species in dehydrated H-ZSM-5 zeolite. In particular, the sensitivity-enhanced 2D $^{31}$P-$^{27}$Al heteronuclear correlation (HETCOR) MAS NMR techniuqe[46] is employed to successfully discriminate the interactions between distinct adsorbed TMPO molecules and Al species in the zeolite framework. Thus, it is straightforward to ascertain the presence of LAS originating from tri-coordinated FAL. Two tri-coordinated FAL species are unambiguously identified by the advanced solid-state NMR technique. Further quantitative NMR analysis reveals that a considerable amount (ca. 11.6%) of this type LAS exists in the framework of dehydrated H-ZSM-5 zeolite even with moderate thermal treatments. Moreover, we demonstrate that the presence of the tri-coordinated FAL is responsible for the formation of superacidity (characterized by a down-field $^{31}$P chemical shift of adsorbed TMPO up to 85-88 ppm) due to the Brønsted/Lewis acid synergy in the zeolite framework which is further confirmed by 2D $^{27}$Al-$^{27}$Al DQ-SQ homonuclear correlation spectroscopy and DFT calculations.


## Results and discussion

### Structure characterization of dehydrated zeolites

The $^{27}$Al MAS NMR spectra of hydrated parent NH$_4$-ZSM-5 acquired at two different magnetic fields (18.8 and 11.4 T) in **Fig. 1a** and **1d** both displayed a typical narrow line around 54 ppm, respectively, corresponding to relatively symmetric tetrahedral Al sites in zeolite framework. Usually much less quadrupolar broadening of the $^{27}$Al NMR lineshape can be obtained at high field ($B_0$ = 18.8 T) and fast MAS speed ($v_R$ = 40 kHz) than that at medium field ($B_0$ = 11.7 T) and moderate
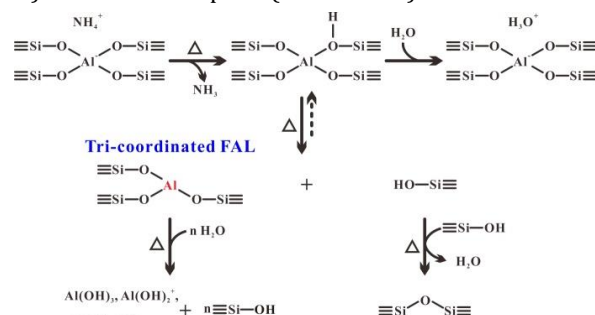


**Scheme 1.** Formation route for tri-coordinated framework Al (FAL) and extra-framework Al (EFAL) species in zeolite.

MAS speed ($\nu_R$ = 10 kHz). While after calcination and dehydration, the $^{27}$Al spectra of dehydrated H-ZSM-5 zeolite exhibited a very broad resonance (**Fig. 1b** and **Fig. 1e**) with a full width of ca. 20 kHz even at 18.8 T, indicative of a dominant contribution from the large second-order quadrupolar broadening. Previous study has demonstrated that this broad signal was mainly attributed to the more-distorted tetrahedral FAL species with a $C_Q \approx$ 16 MHz from Brønsted acidic site on dehydrated zeolites.[35, 36] In fact, dealumination is inevitable in most sample preparation procedures, while the mild vacuum or flow temperature-programmed methods used here couldmake framework dealumination rarely occur, which would largely reduce the interference of EFAL species in the study of tri-coordinated FAL.
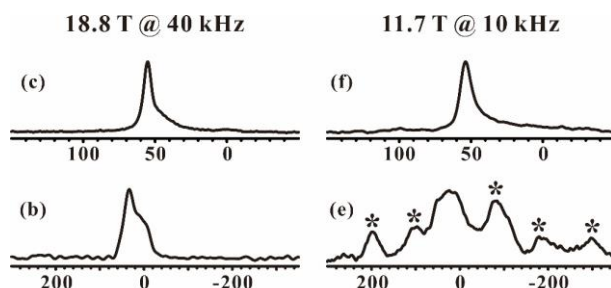


**Figure 1.** 1D $^{27}$Al MAS NMR spectra of parent NH$_4$-ZSM-5 (a and d), calcined and dehydrated H-ZSM-5 (b and e), TMPO-adsorbed H-ZSM-5 with P/Al = 0.42 (c and f), obtained at $B_0$ = 18.8 T (a-c) and $B_0$ = 11.7 T (d-f). The asterisks denote spinning sidebands.
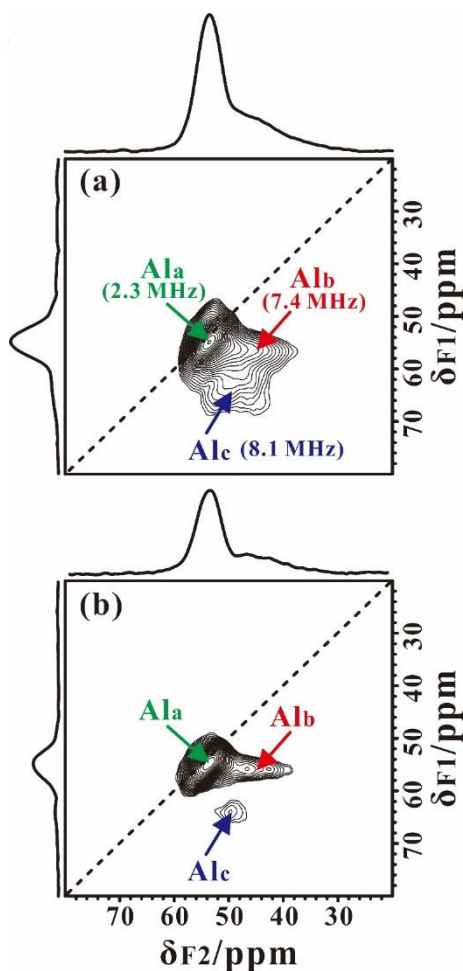


**Figure 2.** Sheared 2D $^{27}$Al 3QMAS NMR spectra of dehydrated H-ZSM-5 zeolites with different TMPO loadings (a) P/Al = 0.42 and (b) P/Al = 0.18, obtained at $B_0$ = 18.8 T. Skyline projections are drawn along F1 and F2. The determined quadrupolar coupling constants are indicated in the brackets for different Al species.

The XRD patterns (**Fig. S1**) of ZSM-5 zeolites indicated no apparent change of crystallinity after these treatments. To estimate the amount of extra-framework Al in our calcined sample, the parent and calcined forms of these zeolites were treated by 1 M aqueous $NaNO_3$ at 353 K for three times. Since the $Na^+$ cations can balance the charge of framework $AlO_4^-$ tetrahedra, the Na/Al ratio is a reliable parameter to assess the variation of fraction of tetrahedral framework Al.[47] The Na/Al ratio measured by ICP was 1.01 and 0.98 respectively for parent $NH_4$-ZSM-5 and dehydrated H-ZSM-5 zeolites treated with $Na^+$ exchange, suggesting that most of the Al species were still located in the zeolite framework. This is also supported by a slight loss (1%) of framework ≡Si-O-Al moieties in the dehydrated zeolite via 1D $^{29}Si$ MAS and 2D $^{29}Si\{^1H\}$ HETCOR NMR analysis (**Fig. S2, S3**). The quantitative $^{29}Si$ MAS spectra in Fig. S3 indicated an increase of Si-OH groups in dehydrated H-ZSM-5 zeolite compared with those in parent $NH_4$-form one. In addition, further $^1H$ MAS NMR analysis (**Fig. S4**) showed that the amount of Si-OH groups decreased when raising the dehyrated temperature from 573 K to 673 K, suggesting that the dehydroxylation of Si-OH groups may occur as depicted in Scheme 1.

## Framework aluminum studied by 2D $^{27}Al$ 3QMAS

In our measurements, TMPO molecules were adsorbed on H-ZSM-5 zeolite with their content much lower than that of framework acid sites, by which the interference between TMPO molecules themselves can be largely avoided. Interestingly, besides the narrow $^{27}Al$ signal at ca. 54 ppm, a new broad shoulder feature (at ca. 45 ppm) was visible in the 1D $^{27}Al$ MAS spectra of dehydrated zeolite loaded with TMPO (P/Al = 0.42, **Fig. 1c, f**). Since the tri-coordinated FAL with Lewis acidity (if present) can directly interact with the oxygen atom of TMPO, which would significantly decrease the asymmetry of the local environment of the Lewis acidic FAL, yielding its "NMR-detectable" $^{27}Al$ resonance on non-hydrated zeolites. Then, 2D $^{27}Al$ 3QMAS experiment at 18.8 T was employed to discriminate specific aluminum sites in the dehydrated and TMPO-loaded sample (**Fig. 2a**). Three signals, denoted as $Al_a$, $Al_b$ and $Al_c$, were well-resolved with the isotropic chemical shifts being 54.4, 51.6 and 58.8 ppm, respectively. For the dehydrated zeolite with a lower TMPO concentration (P/Al= 0.18), an obvious decline of the relative proportion of $Al_c$ and $Al_b$ signals (**Fig.2b, S10**) was evident. The NMR parameters deduced from the 2D spectrum were listed in **Table 1**. The $Al_a$ signal with $P_Q$ = 2.3 MHz could be attributed to the regular tetrahedral FAL species from Brønsted acidic sites analogous to that of $NH_4$-form or hydrated zeolites. The local structure of tetrahedral FAL in dehydrated H-ZSM-5 became more symmetrical stemming from a shrinkage of the Al-O(H) bond length in BAS after TMPO adsorptions. According to their isotropic chemical shifts, $Al_b$ and $Al_c$ should be both associated to tetrahedral FAL species as well, while exhibiting a larger inhomogeneous second-order quadrupolar broadening ($P_Q$ > 7 MHz). However, their assignments were ambiguous, since they could be from either the FAL in another type of BAS, or the tri-coordinated FAL of LAS directly bound to a TMPO molecule, yielding a new distorted tetrahedral FAL state. Especially, the $Al_b$ and $Al_c$ resonances contributed to considerable fraction in the quantitative $^{27}Al$ NMR spectra of dehydrated zeolites with different TMPO loadings (**Fig. 1c**). Therefore, further experiments are required to identify the host-guest correlations/interactions between the adsorbed TMPO probe molecules and the framework of zeolites.

**Table 1.** NMR parameters obtained from $^{27}Al$ MQMAS spectra.

| Site | $\delta_{F2}^a$/ppm | $\delta_{F1}^a$/ppm | $\delta_{CS}^b$/ppm | $P_Q^b$/MHz | $C_Q^c$/MHz |
|------|------|------|------|------|------|
| $Al_a$ | 53.6 | 54.8 | 54.4 | 2.3 | 2.2 |
| $Al_b$ | 44.1 | 56.0 | 51.6 | 7.4 | 7.1 |
| $Al_c$ | 49.7 | 64.1 | 58.8 | 8.1 | 7.8 |

$^a$ $\delta_{F2}$ and $\delta_{F1}$ represent the center of gravity of each particular species measured along direct dimension F2 and isotropic dimension F1 on sheared spectra, respectively.

$^{1b}$ Isotropic chemical shift $\delta_{CS}$, quadrupole interaction product $P_Q$ of each aluminum species were deduced from $\delta_{F2}$ and $\delta_{F1}$.

$^c$ The quadrupolar coupling constant ($C_Q$) were extracted from the slice of 3QMAS spectra by fitting the corresponding second-order quadrupolar lineshape ($\eta$ = 0.5) with the DMFIT program.
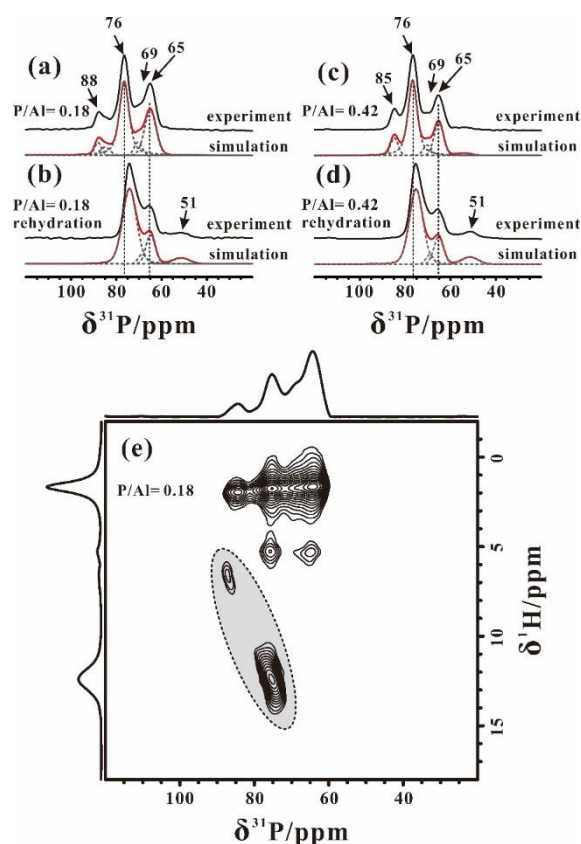
**Figure 3.** 1D one-pulse $^{31}$P MAS spectra of dehydrated H-ZSM-5 zeolites with different TMPO loadings (a,c) and subsequent rehydration (b,d). And 2D $^{31}$P {$^1$H} CP HETCOR MAS NMR spectrum (e) of dehydrated H-ZSM-5 zeolite with a low TMPO loading (P/Al = 0.18).

For the acidity characterization by TMPO probe molecules, the dichloromethane (CH$_2$Cl$_2$) is usually used as the solvent in order to well disperse the TMPO molecules into zeolite.[45, 48] Although the evacuation at 323 K seems to be insufficient to dispose of all solvent, in the 2D $^{13}$C {$^1$H} and $^{31}$P{$^1$H} HETCOR spectra of TMPO/H-ZSM-5 zeolite (**Fig. S5**) acquired with relative short CP contact time (4 ms or 1ms)  there is no correlation between CH$_2$Cl$_2$ and TMPO molecules, indicating that the residual solvent and adsorbed TMPO molecules  are well separated. Furthermore, the $^{27}$Al MAS NMR spectrum of H-ZSM-5 zeolite with solely adsorbed CH$_2$Cl$_2$ (**Fig. S6**) still exhibits a very broad resonance ($\triangle\delta \approx$ 90 ppm), reflecting that the residual CH$_2$Cl$_2$ hardly interacts with acidic sites on zeolite, thus almost has no influence on the acidity characterization by TMPO probe molecules. Note that, after removing the residual solvent on  TMPO/H-ZSM-5 zeolite at a higher temperature (363 K, **Fig. S7**), the $^{27}$Al MAS NMR spectrum of TMPO/H-ZSM-5 was the same as that treated at 323 K (**Fig. S8**), which clearly indicated that the influence of solvent (CH$_2$Cl$_2$) residues on the framework Al species can be negligible.

1D $^{31}$P MAS NMR spectra of H-ZSM-5 zeolites with different TMPO loadings (P/Al = 0.18 and 0.42) were given in **Fig. 3a** and **3c**, respectively. Up to six characteristic peaks at 88, 85, 76, 69, 65 and 51 ppm were identified from the $^{31}$P MAS NMR spectra by using Gaussian deconvolutions (also see **Table S1**). Indeed, quantitative analyses of $^{27}$Al MAS NMR are difficult due to either different quadrupolar broadenings of distinct FAL species or only partial acid sites interacting with TMPO probe molecules, however, here the $^{31}$P (I =1/2) MAS NMR spectra can provide quantitative information on the framework BAS and LAS that react with TMPO molecules. The 2D $^{31}$P {$^1$H} CP-HETCOR spectrum of the TMPO/H-ZSM-5 zeolite (P/Al = 0.18) acquired with a CP contact time of 8 ms in **Fig. 3e** exhibited two broad distributions of correlation peaks in "sloped" oval (dotted line) centered at (76, 12.2) ppm and (88, 6.4) ppm, respectively, which could be assigned to distinct protonated TMPOH$^+$ ionic pair complexes. These correlations were also observable when a short CP contact time (1 ms) was used as (see **Fig. S5**). The interaction of adsorbed TMPO molecules with BAS in H-ZSM-5 zeolite will result in a downfield shift of $^1$H resonance of the acidic proton, and the electron cloud density surrounding the $^{31}$P nucleus in TMPO molecule decreases with increasing acid strength of BAS, leading to the $^{31}$P resonance moved toward higher chemical shift (downfield).[22, 44, 45]

Furthermore, it was also found that the $^{31}$P chemical shift of adsorbed TMPO molecules linearly increases with the increase of Brønsted acid strength, and a $^{31}$P chemical shift of ca. 86 ppm was demonstrated for the threshold of superacidity (with acid strength stronger than 100% H$_2$SO$_4$).[45] Therefore, the $^{31}$P peak at $\delta_{31P}$ = 88 ppm reflected the strongest acid site with strength over the threshold of superacidity in the zeolite. In addition, the correlation peaks between all $^{31}$P signals and methyl groups ($\delta_{1H}$ = 1.8 ppm) of adsorbed TMPO molecules can be observable all the time. Since the $^{1}$H-$^{1}$H spin diffusion will promote the detection of long range interactions in the case of a long CP contact time (8 ms), weak correlations between the protons of the residual CH$_2$Cl$_2$ solvent ($\delta_{1H}$ ≈ 5.4 ppm) and $^{31}$P of TMPO molecules were also detectable in the 2D spectrum.

However, as illustrated in the 2D $^{31}$P {$^{1}$H} HETCOR spectrum of **Fig. 3e**, even though $^{1}$H-$^{1}$H spin diffusion also contributed the $^{1}$H-$^{31}$P correlations when the CP contact time was set to 8 ms, no correlation can be observed for the $^{31}$P signals around 65 ppm with the $^{1}$H signals of BAS, which suggested that the $^{31}$P signals should not originate from the protonated TMPOH$^+$ complexes. It is generally recognized that H$_2$O could competitively react with Lewis acid sites, such as tri-coordinated Al species, to form weak BAS.[48] After exposing our samples to humidity for 2 h, the corresponding $^{31}$P MAS NMR spectra in Fig. 3b, 3d exhibited an apparent decline in relative intensity of the signals at 65 and 69 ppm (also see **Table S1**), and the signal at 88 ppm (or 85 ppm for the sample with P/Al = 0.42) disappeared completely. In addition, the peak at 76 ppm was slightly shifted to upfield with a broader distribution, accompanying a notable increase of the peak at 51 ppm from the TMPO adsorbed on weak acid sites. Therefore, we can reasonably consider that the $^{31}$P signals at 65 ppm and 88 ppm (or 85 ppm) are both associated to Lewis acid sites directly or indirectly. Although the peaks at ca. 88 ppm have proved to be from TMPO molecules adsorbed on Brønsted acid sites, it seems that BAS together with neighboring LAS should contribute to the formation of the superacidity (e.g. $\delta_{31P}$ = 88 ppm), indicative of the presence of synergy effect. Accordingly, after humidity exposure of the dehydrated zeolite, the LAS was preferentially hydrated, thus the influence on its neighboring BAS (the superacid feature) was vanished, which in turn caused the BAS back to its original acidity. The two $^{31}$P signals at 65 and 69 ppm were probably from TMPO molecule adsorbed on Lewis acidic FAL species. Concerning the abundance of Al$_b$ and Al$_c$ in **Fig. 2** (also in **Fig. S10**), we supposed that the aforementioned $^{31}$P and $^{27}$Al species should belong to interacted phosphorus-aluminum pairs in the Lewis acid complexes, (CH$_3$)$_3$PO··Al≡. In addition, we also acquired the 2D $^{31}$P{$^{1}$H} HETCOR spectrum (**Fig. S9**) on the TMPO/H-ZSM-5 zeolite with the complete removal of solvent at 363 K, which exhibited the similar $^{1}$H-$^{31}$P correlations between TMPO molecules and framework acid sites in zeolite compared with that treated at 323 K, which further excluded the influence of residual solvent.
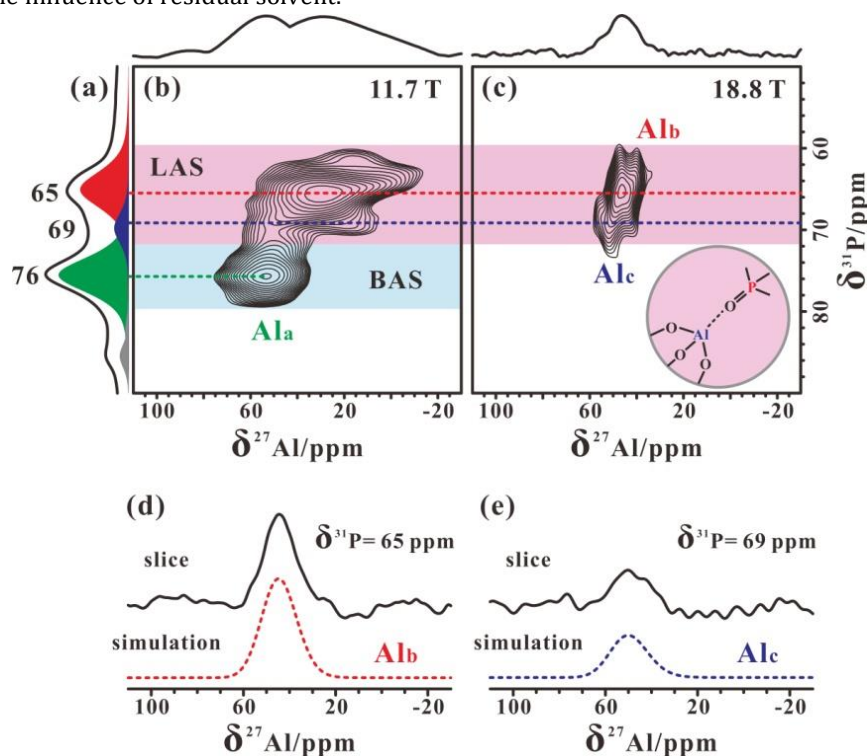


**Figure 4.** 1D one-pulse $^{31}$P MAS (a) and 2D $^{31}$P {$^{27}$Al} PT-D-HMQC MAS (b) NMR spectra recorded at 11.7 T, and 2D $^{27}$Al {$^{31}$P} D-HMQC MAS NMR spectrum (c) recorded at 18.8 T of dehydrated H-ZSM-5 zeolite (Si/Al = 25) with adsorbed TMPO (P/Al = 0.42). Selected slices with simulations are shown on (d) and (e).

## Tri-coordinated framework Al characterized by [31]P {[27]Al} HMQC and [31]P {[27]Al} S-RESPDOR

To verify the assumption, the Lewis complex $(CH_3)_3PO \cdot \cdot Al \equiv$ was identified directly by using our recently developed [31]P-[27]Al population-transfer dipolar-mediated HMQC (PT-*D*-HMQC) experiment which can establish the direct correlation/ connectivity between TPMO and various Al species. As shown in Fig. S5, the 1D ^{31}P {^{27}Al} PT-*D*-HMQC MAS NMR spectra via [31]P→[27]Al→[31]P filtering on TMPO-loaded H-ZSM-5 zeolite (P/Al = 0.42) revealed that the two main ^{31}P resonances around 76 and 65 ppm were correlated with [27]Al species in zeolite. When using a short recoupling time ($\tau_{mix}$ = 1.33 ms), the peaks at ca. 65 ppm became more intense compared to that at ca. 76 ppm (**Fig. S11**). This indicated the stronger [31]P-[27]Al dipolar interaction of corresponding spin pairs, further suggesting the presence of the Lewis complex $[(CH_3)_3PO \cdot \cdot Al \equiv]$.

Notably, the 2D [31]P {[27]Al} PT-*D*-HMQC spectrum acquired at 11.7 T of TMPO-adsorbed H-ZSM-5 zeolite in **Fig. 4b** clearly illustrated two correlation groups. The correlation peak at around (76, 54) ppm was associated with TMPO adsorbed on the bridging hydroxyl (Si-OH-Al) proton (*i.e.* Brønsted acid sites). Importantly, other correlations indicated that the ^{31}P resonance peaks at 65 and 69 ppm are both correlated with broad [27]Al resonances from distorted four-coordinated aluminum, reflecting the presence of two types of Lewis acid sites. We also conducted 2D [27]Al {[31]P} *D*-HMQC experiments at 18.8 T. Due to the short transverse relaxation times ($T_2$) of [27]Al resonances, we could only observe [27]Al-^{31}P correlations from the Lewis complex $[(CH_3)_3PO \cdot \cdot Al \equiv]$ in **Fig. 4c**, in which ^{31}P signals at 65 and 69 ppm were correlated with $Al_b$ and $Al_c$, respectively (**Fig. 4d, 4e**). Meanwhile, a reduction of the TMPO concentration led to a decrease in the proportion of ^{31}P signal at 69 ppm relative to that at 65 ppm (**Table S1**), in consistent with the relative proportion variation of $Al_c$ and $Al_b$ (**Fig. 2**). Therefore, we can confirm that $Al_c$ and $Al_b$ are both from tri-coordinated FAL species bound to the O atom of TMPO molecules, which were well discriminated from their different Lewis acid strength.

Due to its low content and Brønsted acid feature, we didn't observe the [31]P-[27]Al correlations from the ^{31}P signal at 88 ppm (or 85 ppm) in **Fig. 4**. Fortunately, Symmetry-based Resonance-Echo Saturation-Pulse DOuble-Resonance (S-RESPDOR) method[49] can be employed here to estimate [31]P-[27]Al heteronuclear dipolar interactions. The results are usually analyzed by plotting the signal fraction $\Delta S/S_0 = (S_0 - S')/S_0$ ($S'$ and $S_0$ represent the signal intensity with and without dipolar dephasing, respectively) as function of the recoupling time $\tau$. The difference ^{31}P spectrum ($\Delta S = S_0 - S'$, shown in **Fig. S12**) obtained by
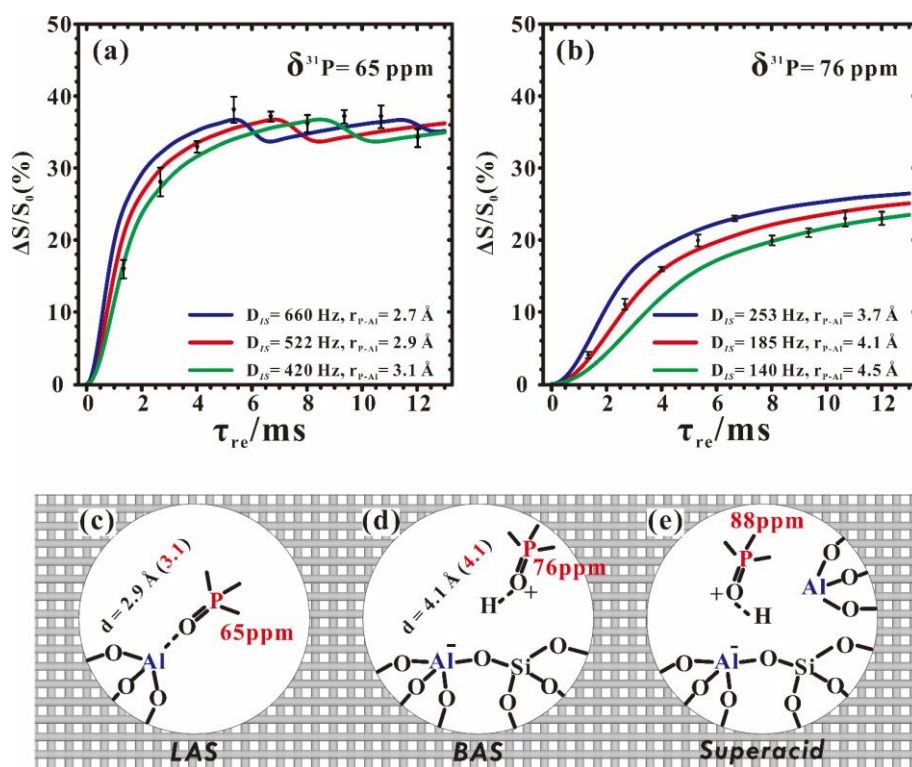


**Figure 5.** [31]P {[27]Al} S-RESPDOR built-up curves of TMPO adsorbed on (a) LAS (tri-coordinated FAL) and (b) BAS of dehydrated H-ZSM-5 zeolite, fitted by analytical formula. $D_{IS}$ and $r_{P–Al}$ represent the dipolar interaction constant and internuclear distance of the [31]P-[27]Al spin pair, respectively. And three adsorption structure models of (c) TMPO adsorbed on tri-coordinated FAL, forming a distorted tetrahedral FAL, (d) TMPO adsorbed on Brønsted acid site, and (e) TMPO adsorbed on Brønsted acid site with tri-coordinated FAL in close proximity. The red numbers in the parentheses were the distances obtained by DFT calculations.

1D [31]P {[27]Al} S-RESPDOR experiments still suggested the spatial interactions/proximities between all ^{31}P species of adsorbed TMPO molecules (including that giving rise to the resonance at 88 ppm) and [27]Al species in the framework of H-ZSM-5. Furthermore, the lower concentration of TMPO molecules (P/Al = 0.18) allowed us to estimate distances between ^{31}P atoms

and $^{27}$Al atoms, since we could approximately consider the Lewis complex [(CH$_3$)$_3$PO··Al≡] with $^{31}$P signals at 65 ppm or Brønsted acid complex [(CH$_3$)$_3$PO··H-OAl≡] with $^{31}$P signals at 76 ppm as "isolated" phosphor–aluminum spin pairs in this case. Therefore, the P-Al distance of the former was determined to be 2.9 ± 0.2 Å by fitting the dephasing curve (**Fig. 5a**), which was rationalized in terms of the structure model of TMPO molecule adsorbed on the framework tri-coordinated aluminum species (**Fig. 5c**). While the later complex had a reasonable P-Al distance of 4.1± 0.4 Å (**Fig. 5b**), in which $^{31}$P atom was about four bonds away from the Al site (**Fig. 5d**). We also considered the dipolar coupling networks of multiple-spin systems (shown in **Fig. S13**). The representative three spin system are depicted in **Fig. S13b-d**. In the normalized dipolar dephasing curve with respect to first extremum (or maximum) in each spin system, it is found that the dephasing curves of the observed $^{31}$P signals in multi-spin systems have similar upward trend to that of the isolated $^{31}$P-$^{27}$Al spin pair. This result suggests that the upward trend of the dipolar dephasing curve is dominated by the short-range (strongest) $^{31}$P-$^{27}$Al dipolar interaction. The long-range couplings have little impact on the measurement of the short distance, which mainly affect the oscillation of the dephasing curves after reaching its first extremum. Moreover, the $^{31}$P-$^{27}$Al distances extracted by the dipolar dephasing curves were in good agreement with DFT calculations, where the theoretically predicted $^{31}$P-$^{27}$Al distances of the Lewis acid complex [(CH$_3$)$_3$PO··Al≡] and Brønsted acid complex [(CH$_3$)$_3$PO··H-OAl≡] were 3.1 Å and 4.1 Å (**Fig. 5c and 5d**)，respectively.

Although it is difficult to calculate the accurate amount of the tri-coordinated FAL in our sample, an estimation of the lower limit of their concentration via the quantitative analysis of $^{31}$P MAS NMR spectrum (**Fig. 3**) is available with the following equation:

$$\Omega(FAL^{III}) = \chi(P/Al) * \Omega(^{31}P_{LAS})$$

Where $\Omega(FAL^{III})$ is the fraction of tri-coordinated FAL species interacted with TMPO in the total Al content, $\Omega(^{31}P_{LAS})$ = 27.0% is the proportion of $^{31}$P signals at 65 and 69 ppm in the quantitative $^{31}$P MAS NMR spectrum (see **Table S1**), and $\chi(P/Al)$ = 0.42 is the atomic ratio of P to Al of the sample obtained by ICP. Therefore, the calculated $\Omega(FAL^{III})$ = 11.6% suggested that a considerable amount of LAS formed and located in the framework of dehydrated H-ZSM-5 zeolite, in agreement with the relative content of Lewis acid sites (13.3%) determined by our FT-IR analysis of pyridine adsorption measurements (**Table 2** and **Fig. S14**).

**Table 2.** Concentration of BAS and LAS on H-ZSM-5 (Si/Al = 25) samples.

| Sample | $n$(BAS+LAS)$^a$ μmol/g | $n$(BAS)$^b$ μmol/g | $n$(LAS)$^c$ μmol/g |
|---|---|---|---|
| H-ZSM-5/25 | 647.2 | 511.4 | 86.1 |

$^a$ calculated by ICP-OES. $^b$ determined by $^1$H MAS NMR. $^c$ calculated from pyridine-FTIR.
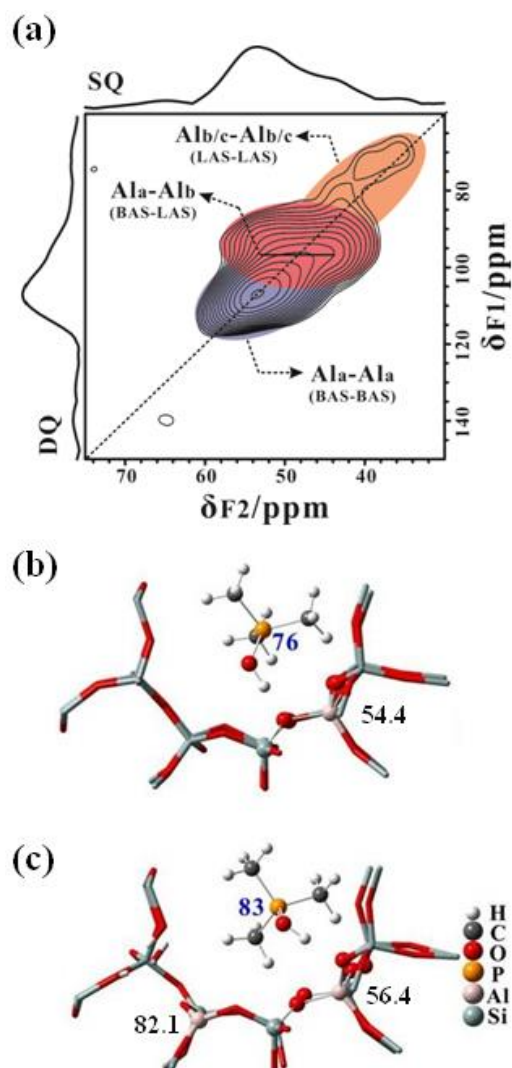
**Figure 6.** 2D $^{27}Al$-$^{27}Al$ DQ-SQ MAS NMR spectra (a) of dehydrated and TMPO-loaded H-ZSM-5 zeolite (P/Al = 0.42), recorded at 18.8 T with a spinning speed of 20 kHz. Local theoretically optimized structures of TMPO adsorbed at the isolated Brønsted site (b) and Brønsted/Lewis acid synergetic site (c) with tri-coordinated framework Al in close proximity. The predicted $^{31}P$ chemical shifts of TMPO (blue numbers) and $^{27}Al$ chemical shifts of corresponding acid sites (black numbers) were labeled in ppm.

## Brønsted/Lewis synergy effect studied by 2D $^{27}Al$ DQ-SQ NMR and DFT calculations

We have successfully obtained the high-resolution $^{27}Al$-$^{27}Al$ DQ-SQ homonuclear correlation spectra on hydrated zeolites (HY, MOR, ZSM-5, *etc.*) by using our developed BR2$^1_2$ recoupling scheme at high magnetic field,[32, 41] whereas only Al species from framework BAS and extra-framework LAS were considered. In the case of non-hydrated zeolite catalysts, the broadening and overlap of the $^{27}Al$ quadrupolar patterns usually result in considerable barriers to implementation of the 2D $^{27}Al$ DQ-SQ experiment. Fortunately, the improved resolution of $^{27}Al$ MAS NMR spectra of dehydrated H-ZSM-5 zeolite after TMPO adsorptions offers an opportunity to investigate the intrinsic structure of different framework Al species under dehydrated state, whose acidic natures have been clearly characterized. **Fig. 6a** displayed the $^{27}Al$-$^{27}Al$ DQ-SQ MAS NMR spectrum of TMPO-adsorbed H-ZSM-5 with P/Al = 0.42 at 18.8 T. Two auto-correlation peaks were observable, in which the intense blue part indicated that tetra-coordinated framework Al species ($Al_a$) was in close proximity one another ($Al_a$), and the weak orange part was ascribed to the spatial proximity of $Al_b$-$Al_b$ or $Al_c$-$Al_c$ pairs in a low content. Note that, it is still hard to discriminate the $Al_b$ and $Al_c$ in the $^{27}Al$ DQ-SQ MAS NMR spectrum. In addition, the appearance of an intense cross-peak pair between $Al_a$ and $Al_b$ (Red part in **Fig. 6**) provided a direct evidence on the spatial proximity between the framework Brønsted and Lewis acid sites, where $Al_a$ and $Al_b$ had been confirmed from the Brønsted acid complex [(CH$_3$)$_3$PO··H-OAl≡] and Lewis acid complex [(CH$_3$)$_3$PO··Al≡] in the TMPO-loaded H-ZSM-5, respectively. Therefore, it implied that the

superacidity characterized by $^{31}$P NMR signals at 85-88 ppm (**Fig. 3**) on the specific BAS should be derived from the influence of the neighboring tri-coordinated FAL (LAS), generating a Brønsted/Lewis synergy effect. The assignment was also confirmed by the absence of the $^{31}$P signals at 85-88 ppm on a quantitatively TMPO-adsorbed H-ZSM-5 zeolite with a low Si/Al of 140 (see **Fig. S15**), which has a much less probability of Al-Al pair in close proximity in the zeolite framework due to the much lower Al content.

In order to gain more insights into the Brønsted/Lewis synergy effect, we also performed DFT calculations (see **Fig. S16**). As shown in the local theoretically optimized structures (**Fig. 6b** and **6c**), for TMPO adsorbed on the BAS with a neighboring tri-coordinated FAL site, a $^{31}$P chemical shift of 83 ppm was theoretically predicted, while for TMPO adsorbed on the isolated BAS, a $^{31}$P chemical shift of 76 ppm was achieved, in consistence with our experimental observation. The calculated $^{31}$P and $^{27}$Al isotropic chemical shifts for different adsorption models were listed in **Table S3**. Except for the unreacted "NMR-invisible" framework LAS (tri-coordinated FAL), the chemical shift parameters extracted from DFT calculations were in consistence with our experimental results. These results indicate that the synergistic effect between framework BAS and framework LAS (tri-coordinated FAL) due to their spatial proximity (**Fig. 5e**) leads to an enhancement of Brønsted acidity and thus generates the superacidity in H-ZSM-5 zeolite.

## Conclusions

Tri-coordinated framework aluminum species can also serve as Lewis acid sites in principle, however, one of fundamental challenges is to observe and distinguish these tri-coordinated framework aluminum species in zeolite. Their relatively low concentration and largely distorted local environment make them "NMR-invisible" in zeolites, thus the experimental study on their acidic property is rarely reported. Benefiting from the current state-of-the-art multi-nuclear and multi-dimensional solid-state NMR spectroscopy, unique insights into the structure and property of tri-coordinated FAL species acting as Lewis acid sites in H-ZSM-5 have been achieved in conjunction with TMPO probe molecule adsorptions. Since the unsaturated tri-coordinated FAL species can act with the basic TMPO probe molecules to form distorted tetrahedral FAL sites, two tri-coordinated FAL species with different Lewis acidities were discriminated by sensitivity-enhanced 2D $^{31}$P-$^{27}$Al *D*-HMQC MAS NMR experiments. In particular, the adsorption models of TMPO probe molecules on distinct acidic sites in H-ZSM-5 were clearly illustrated, and the strong $^{31}$P-$^{27}$Al dipolar interaction from the Lewis complex [(CH$_3$)$_3$PO··Al≡] was confirmed by measuring the distance between corresponding $^{31}$P and $^{27}$Al atoms. Furthermore, the remarkably improved resolution and sensitivity of $^{27}$Al MAS NMR spectrum of TMPO-adsorbed H-ZSM-5 zeolite allowed us to obtain a well-resolved 2D $^{27}$Al DQ-SQ homonuclear correlation spectrum, and thus to understand the structure of different framework acid sites in non-hydrated zeolite. Consequently, the superacidity of BAS (with acid strength stronger than 100% H$_2$SO$_4$) induced by the synergy effect between framework BAS and framework LAS (tri-coordinated FAL) was evidenced by their close spatial proximity in dehydrated H-ZSM-5 zeolites and the observation of $^{31}$P chemical shift up to 85-88 ppm for adsorbed TMPO. Notably, apart from the extra-framework Al as LAS in zeolite, the existence of considerable amount of tri-coordinated framework Al serving as LAS in zeolite framework suggests that further studies are needed to understand its catalytic function, which might be essential to rationally design highly efficient zeolite catalysts. The detailed characterizations of tri-coordinated framework Al in H-ZSM-5 in this work provide a useful strategy to explore the acidic nature of this type of "moisture-sensitive" species in zeolite catalysts, which may shed light on experimental exploration of its structure-function relationship in zeolite catalysis.

## Experimental section

### Sample preparations

Parent NH$_4$-ZSM-5 with Si/Al = 25 and Si/Al =140 was purchased from Zeolyst International. The sample was calcined at 773 K under a dry air atmosphere for 10 h to remove the template and the H-form of ZSM-5 was obtained. Prior to adsorption of TMPO, the sample was dehydrated on a vacuum line. The temperature was gradually increased at a rate of 1 °C min$^{-1}$ and the sample was kept at a final temperature of 673 K at a pressure below 10$^{-3}$ Pa overnight. Detailed procedures involved in introducing the TMPO probe molecule onto the sample can be found elsewhere.[45] In brief, a known amount of TMPO dissolved in anhydrous CH$_2$Cl$_2$ was first added into a vessel containing the dehydrated H-ZSM-5 sample in a N$_2$ glovebox, followed by removal of the CH$_2$Cl$_2$ solvent by evacuation on a vacuum line at 323 K or 363 K. To ensure a uniform adsorption of TMPO molecules in the pores/channels of the zeolites, the sealed vessel was further subjected to a thermal treatment at 453 K for 2 h. Finally, the sample was transferred into a ZrO$_2$ MAS rotor in the N$_2$ glovebox prior to the solid-state NMR experiments.

### ICP experiment

Atomic emission spectroscopy (AES-ICP) was used to determine the relative amounts of silicon, aluminum and phosphorus in TMPO-loaded H-ZSM-5 samples. Na and Al contents were measured by AES-ICP for a 10 mg sample dissolved in 50 mL HF solution.

## FT-IR of pyridine adsorption

FT-IR of pyridine adsorption measurements were conducted on a Bruker Tensor 27 spectrometer. About 20 mg sample was pressed into a self-supported wafer with a diameter of 13 mm. Prior to the measurement, the catalysts were evacuated to $10^{-2}$ Pa at 673 K for 2 h. After cooling down to room temperature, pyridine vapor was introduced into the sample cell at room temperature for 30 min to allow equilibrium, the residual pyridine was removed by vacuum. The FT-IR spectra of pyridine-adsorbed samples were measured at 423, 523, and 623 after evacuation for 30 min, respectively.

## Solid-state NMR experiments

For all 2D HETCOR experiments, the isotope within the braces represents that it is indirectly detected in F1 dimension. 1D $^1$H MAS NMR and $^{31}$P MAS NMR experiments were performed on an 9.4 T Bruker AVANCE-Ⅲ spectrometer using 4 mm rotors at a spinning frequency of 10 kHz (operating at a Larmor frequency of 399.3 MHz and 161.7 MHz, respectively). The $^1$H single-pulse acquisition was employed with a pulse width of 3.9 $\mu$s (ca. $\pi/2$ pulse), a recycle delay of 3 s, and 32 scans. The $^{31}$P single-pulse acquisition was employed with a pulse width of 3 $\mu$s (ca. $\pi/2$ pulse), a recycle delay of 30 s, and 1024 scans, in which the RF amplitude of $^1$H TPPM decoupling was set to ca. 50 kHz.

The $^{29}$Si MAS NMR experiments were performed on an 11.7 T Bruker AVANCE-Ⅲ spectrometer using 7 mm rotors at a spinning frequency of 6 kHz (operating at a Larmor frequency of 99.4 MHz). The $^{29}$Si single-pulse acquisitions were employed with a pulse width of 8.4 $\mu$s (ca. $\pi/2$ pulse), a recycle delay of 30 s, and 320 scans, in which the RF amplitude of $^1$H TPPM decoupling was set to ca. 38 kHz.

The single-pulse $^{27}$Al MAS NMR data were collected on an 11.7 T Bruker AVANCE-Ⅲ spectrometer with a 4 mm double-resonance probe at a spinning rate of 10 kHz, a pulse width of 0.4 $\mu$s (ca. $\pi/6$ pulse), a recycle delay of 1 s, and 2048 scans. To improve resolution, the single-pulse $^{27}$Al MAS NMR data were also collected on an 18.8 T Bruker AVANCE-Ⅲ spectrometer (corresponding to a $^{27}$Al Larmor frequency of 208.6 MHz) with an 1.9 mm double-resonance probe at a spinning rate of 40 kHz, a pulse width of 0.3 $\mu$s (ca. $\pi/9$ pulse), a recycle delay of 1 s, and 4096 scans.

The 2D $^{27}$Al triple-quantum (3Q) MAS z-filtering NMR experiments with fast amplitude modulation (FAM) enhancement[50] were also carried out at 18.8 T. The pulse duration were set to 3.6 $\mu$s for the first strong pulse with $\nu_{RF} \approx 125$ kHz. A FAM pulse train consist of 4 loops of two short pulses ($\nu_{RF} \approx 125$ kHz) and two delays with the same duration of 0.7 $\mu$s to convert $p = \pm 3$ to $\pm 1$ coherences. The "soft" $\pi/2$ pulses were set to 10.4 $\mu$s.

The 1D $^{31}$P $\{^{27}$Al$\}$ S-RESPDOR and 2D $^{31}$P $\{^{27}$Al$\}$ PT-$D$-HMQC MAS NMR experiments were performed on an 11.7 T Bruker AVANCE-Ⅲ spectrometer using commercial 7 mm rotors with an o-ring cap at a spinning frequency of 6 kHz, tuning and matching to $^1$H, $^{31}$P and $^{27}$Al Larmor frequencies (500.6 MHz, 202.6 MHz and 130.5 MHz, respectively). $^1$H-$^{31}$P CP with a contact time of 8 ms was employed to prepare the initial $^{31}$P signal.

For $^{31}$P $\{^{27}$Al$\}$ S-RESPDOR experiments, a saturation pulse on the $^{27}$Al channel with amplitude of ca. 25 kHz and a length of 166.67 $\mu$s ($T_R$) was irradiated at ca. 30 ppm to transfer $^{31}$P-$^{27}$Al interactions. For 2D $^{31}$P $\{^{27}$Al$\}$ PT-$D$-HMQC experiments, repetitive sideband-selective (SS) WURST-80 adiabatic pulses with a length 166.67 $\mu$s were employed on Al channel during SR4 recoupling to accelerate coherence transfers between $^{31}$P and $^{27}$Al. The values for peak RF amplitude and offset of WURST-80 were optimized with ($\nu_1^{max}$, $\nu_{offset}$) = (7.5, 175) kHz on $^{27}$Al channel. For 2D $^{27}$Al $\{^{31}$P$\}$ $D$-HMQC and $^{27}$Al DQ-SQ MAS NMR experiments, central transition (CT) enhancement of the initial magnetizations ($^{27}$Al) was obtained by using a SS-WURST-80 irradiation with a length of 1 ms. More details on the NMR parameters of 2D or double-resonance experiments can be found in Table S2.

All simulations of 1D MAS NMR spectra or slices were performed with the DMFIT software.[51] The chemical shift for $^1$H, $^{31}$P, $^{29}$Si and $^{27}$Al were referenced to adamantane, 85% $H_3PO_4$, kaolinite and 1 M aqueous Al(NO3)$_3$, respectively.

## DFT Calculations

All the structures of ZSM-5 zeolite are represented by a 64 T model (containing the complete double 10-membered ring (MR) intersection pores formed by 10-MR straight and 10-MR sinusoidal pore channels), which were extracted from their crystallographic structural data (**http://www.iza-structure.org/databases/**). The terminal Si–H was fixed at a bond length of 1.47 Å, oriented along the direction of the corresponding Si–O bond. The geometries of TMPO adsorbed at the isolated Brønsted acid site and the Brønsted/Lewis synergetic site of ZSM-5 were optimized over the 64 T cluster model by the combined theoretical ONIOM method. In the calculations, the TMPO and the high layer atoms of the zeolite framework were allowed to fully relax with the dispersion-corrected ωB97XD functional[52] with 6-31G(d, p) basis set, whereas the rest atoms were fixed at their crystallographic positions with AM1 method. Based on the optimized structures, the $^{31}$P and $^{27}$Al NMR chemical shifts were then calculated at the ωB97XD/TZVP level by GIAO method.

## Conflicts of interest

The authors declare no conflict of interest.

## Acknowledgements

## References

1. J. Biswas and I. E. Maxwell, *Appl Catal*, 1990, **63**, 197-258.
2. M. Moliner, Y. Roman-Leshkov and M. E. Davis, *Proc. Nat. Acad. Sci. U.S.A.*, 2010, **107**, 6164-6168.
3. A. Corma, V. Martínez-Soria and E. Schnoeveld, *J. Catal.*, 2000, **192**, 163-173.
4. J. Wahlen, S. Dehertogh, D. Devos, V. Nardello, S. Bogaert, J. Aubry, P. Alsters and P. Jacobs, *J. Catal.*, 2005, **233**, 422-433.
5. A. Vjunov, J. L. Fulton, T. Huthwelker, S. Pin, D. H. Mei, G. K. Schenter, N. Govind, D. M. Camaioni, J. Z. Hu and J. A. Lercher, *J. Am. Chem. Soc.*, 2014, **136**, 8296-8306.
6. T. Y. Liang, J. L. Chen, Z. F. Qin, J. F. Li, P. F. Wang, S. Wang, G. F. Wang, M. Dong, W. B. Fan and J. G. Wang, *ACS Catal.*, 2016, **6**, 7311-7325.
7. K. Z. Chen, M. Abdolrhamani, E. Sheets, J. Freeman, G. Ward and J. L. White, *J. Am. Chem. Soc.*, 2017, **139**, 18698-18704.
8. H. M. Kao, C. P. Grey, K. Pitchumani, P. H. Lakshminarasimhan and V. Ramamurthy, *J. Phys. Chem. A*, 1998, **102**, 5627-5638.
9. S. M. Maier, A. Jentys and J. A. Lercher, *J. Phys. Chem. C*, 2011, **115**, 8005-8013.
10. W. O. Haag, R. M. Lago and P. B. Weisz, *Nature*, 1984, **309**, 589-591.
11. S. H. Li, A. M. Zheng, Y. C. Su, H. L. Zhang, L. Chen, J. Yang, C. H. Ye and F. Deng, *J. Am. Chem. Soc.*, 2007, **129**, 11161-11171.
12. D. E. Perea, I. Arslan, J. Liu, Z. Ristanovic, L. Kovarik, B. W. Arey, J. A. Lercher, S. R. Bare and B. M. Weckhuysen, *Nat. Commun.*, 2015, **6**, 7589.
13. H. Koller, T. Uesbeck, M. R. Hansen and M. Hunger, *J. Phys. Chem. C*, 2017, **121**, 25930-25940.
14. C. Schroeder, M. R. Hansen and H. Koller, *Angew. Chem. Int. Ed.*, 2018, **57**, 14281-14285.
15. M. Milina, S. Mitchell, P. Crivelli, D. Cooke and J. Perez-Ramirez, *Nat. Commun.*, 2014, **5**, 3922.
16. Z. Wang, L. Wang, Y. Jiang, M. Hunger and J. Huang, *ACS Catal.*, 2014, **4**, 1144-1147.
17. S. Prodinger, M. A. Derewinski, A. Vjunov, S. D. Burton, I. Arslan and J. A. Lercher, *J. Am. Chem. Soc.*, 2016, **138**, 4408-4415.
18. I. Yarulina, K. De Wispelaere, S. Bailleul, J. Goetze, M. Radersma, E. Abou-Hamad, I. Vollmer, M. Goesten, B. Mezari, E. J. M. Hensen, J. S. Martinez-Espin, M. Morten, S. Mitchell, J. Perez-Ramirez, U. Olsbye, B. M. Weckhuysen, V. Van Speybroeck, F. Kapteijn and J. Gascon, *Nat. Chem.*, 2018, **10**, 804-812.
19. R. Weingarten, G. A. Tompsett, W. C. Conner and G. W. Huber, *J. Catal.*, 2011, **279**, 174-182.
20. M. Orazov and M. E. Davis, *Chemical science*, 2016, **7**, 2264-2274.
21. P. Batamack, C. Doremieuxmorin, R. Vincent and J. Fraissard, *Microporous Mater.*, 1994, **2**, 515-524.
22. A. Zheng, S. Li, S. B. Liu and F. Deng, *Acc Chem Res*, 2016, **49**, 655-663.
23. Y. Y. Chu, X. F. Yi, C. B. Li, X. Y. Sun and A. M. Zheng, *Chemical science*, 2018, **9**.
24. A. Zecchina, S. Bordiga, G. Spoto, D. Scarano, G. Petrini, G. Leofanti, M. Padovan and C. O. Arean, *J. Chem. Soc., Faraday Trans.*, 1992, **88**, 2959-2969.
25. F. Collignon, P. A. Jacobs, P. Grobet and G. Poncelet, *J. Phys. Chem. B*, 2001, **105**, 6812-6816.
26. J. A. van Bokhoven, A. M. J. van der Eerden and D. C. Koningsberger, *J. Am. Chem. Soc.*, 2003, **125**, 7435-7442.
27. W. P. Zhang, S. T. Xu, X. W. Han and X. H. Bao, *Chem. Soc. Rev.*, 2012, **41**, 192-210.
28. S. E. Ashbrook and S. Sneddon, *J. Am. Chem. Soc.*, 2014, **136**, 15440-15456.
29. Z. C. Wang, Y. J. Jiang, O. Lafon, J. Trebosc, K. D. Kim, C. Stampfl, A. Baiker, J. P. Amoureux and J. Huang, *Nat. Commun.*, 2016, **7**, 13820.
30. C. Coperet, W. C. Liao, C. P. Gordon and T. C. Ong, *J. Am. Chem. Soc.*, 2017, **139**, 10588-10596.
31. D. Xiao, S. T. Xu, X. W. Han, X. E. Bao, Z. M. Liu and F. Blanc, *Chemical science*, 2017, **8**, 8309-8314.
32. Z. W. Yu, A. M. Zheng, Q. Wang, L. Chen, J. Xu, J. P. Amoureux and F. Deng, *Angew. Chem. Int. Ed.*, 2010, **49**, 8657-8661.
33. J. Brus, L. Kobera, W. Schoefberger, M. Urbanova, P. Klein, P. Sazama, E. Tabor, S. Sklenak, A. V. Fishchuk and J. Dedecek, *Angew. Chem. Int. Ed.*, 2015, **54**, 541-545.
34. C. P. Grey and A. J. Vega, *J. Am. Chem. Soc.*, 1995, **117**, 8232-8242.
35. A. P. M. Kentgens, D. Iuga, M. Kalwei and H. Koller, *J. Am. Chem. Soc.*, 2001, **123**, 2925-2926.
36. J. Jiao, J. Kanellopoulos, W. Wang, S. S. Ray, H. Foerster, D. Freude and M. Hunger, *Phys. Chem. Chem. Phys.*, 2005, **7**, 3221-3226.
37. P. A. Jacobs and H. K. Beyer, *J. Phys. Chem.*, 1979, **83**, 1174-1177.
38. Q. L. Wang, G. Giannetto, M. Torrealba, G. Perot, C. Kappenstein and M. Guisnet, *J. Catal.*, 1991, **130**, 459-470.
39. G. L. Woolery, G. H. Kuehl, H. C. Timken, A. W. Chester and J. C. Vartuli, *Zeolites*, 1997, **19**, 288-296.
40. E. Lam, A. Comas-Vives and C. Copéret, *J. Phys. Chem. C*, 2017, **121**, 19946-19957.

41. Z. W. Yu, S. H. Li, Q. Wang, A. M. Zheng, X. Jun, L. Chen and F. Deng, *J. Phys. Chem. C*, 2011, **115**, 22320-22327.

42. X. F. Yi, K. Y. Liu, W. Chen, J. J. Li, S. T. Xu, C. B. Li, Y. Xiao, H. C. Liu, X. W. Guo, S. B. Liu and A. M. Zheng, *J. Am. Chem. Soc.*, 2018, **140**, 10764-10774.

43. J. F. Haw, J. B. Nicholas, T. Xu, L. W. Beck and D. B. Ferguson, *Acc. Chem. Res.*, 1996, **29**, 259-267.

44. E. F. Rakiewicz, A. W. Peters, F. Wormsbecher, K. J. Sutovich and K. T. Mueller, *J. Phys. Chem. B*, 1998, **102**, 2890-2896.

45. A. Zheng, S. B. Liu and F. Deng, *Chem Rev*, 2017, **117**, 12475-12531.

46. Q. Wang, Y. X. Li, J. Trebosc, O. Lafon, J. Xu, B. W. Hu, N. D. Feng, Q. Chen, J. P. Amoureux and F. Deng, *J. Chem. Phys.*, 2015, **142**.

47. A. Janda and A. T. Bell, *J. Am. Chem. Soc.*, 2013, **135**, 19193-19207.

48. Q. Zhao, W. H. Chen, S. J. Huang, Y. C. Wu, H. K. Lee and S. B. Liu, *J. Phys. Chem. B*, 2002, **106**, 4462-4469.

49. L. Chen, X. Y. Lu, Q. A. Wang, O. Lafon, J. Trebosc, F. Deng and J. P. Amoureux, *J. Magn. Reson.*, 2010, **206**, 269-273.

50. P. K. Madhu, A. Goldbourt, L. Frydman and S. Vega, *Chem. Phys. Lett.*, 1999, **307**, 41-47.

51. D. Massiot, F. Fayon, M. Capron, I. King, S. Le Calve, B. Alonso, J. O. Durand, B. Bujoli, Z. H. Gan and G. Hoatson, *Magn. Reson. Chem.*, 2002, **40**, 70-76.

52. J. D. Chai and M. Head-Gordon, *J. Chem. Phys.*, 2008, **128**.